Finite element analysis of laser transformation hardening

J. Huétink, L.H.J.F. Beckmann, H.J.M. Geijselaers

University of Twente, Faculty of Mechanical Engineering
P.O.Box 217, 7500 AE Enschede, The Netherlands

ABSTRACT

The problem of determining stresses, phase compositions and temperature distributions during the transformation hardening of steel with a CO_2-laser beam is investigated.
To model the different phases in each material point a parallel fraction model is used, in which each fraction represents one phase.
The description of phase transformations is obtained by an incremental formulation of the Avrami-equation for isothermal transformation.
A model is developed to describe the superheating of ferrite and pearlite. The model is demonstrated by a detailed computation of stresses, deformations and phase compositions in the case of a stationary laser flash.

1. INTRODUCTION

The conventional hardening of steel is done by heating the whole product to a temperature above Ac3 ($\approx$ 800 $^{\circ}$C), where all the ferrite and pearlite is allowed to transform to austenite. Quenching in water or oil will result in rapid cooling of the product. Part of the austenite is maintained until below the Ms temperature (martensite start 250°C - 550°C, depending on chemical composition). This will then transform to martensite, which gives the desired hardening.
With laser hardening however, heat is applied locally, using a laser beam. The temperature rises very rapidly to almost melting temperature. Only a thin layer is heated, the other parts of the product remain cold. Due to the high temperature gradients, thermal conduction to the cold bulk material will cause sufficiently rapid cooling of the heated parts and most of the austenite, that is formed during heating, will transform to martensite[1].
The process involves extremely high heating and cooling rates (10^3 - 10^6 K/s). Also, the interaction time is very short ($\approx$ 1s).
As a result, compared to conventional hardening, less energy is needed, the grain sizes are smaller and there is less risk of distortion of the product.
One of the complications is, that due to the short interaction time not all of the ferrite and pearlite in the heated region are allowed to transform to austenite. A considerable superheating of ferrite may occur. One object of this paper is to show how this phenomenon may be modeled.

2. PHASE TRANSFORMATIONS

2.1. Diffusion controlled transformations

The equilibrium phase composition at different temperatures can be read from the equilibrium phase diagram (Fig. 1.). Some of the transitions between different phases require diffusion of carbon. This means in general, that these transitions take some time to materialize. The kinetics are governed by the Avrami equation[2], which is a solution to the diffusion equation and takes into account, the time

required for nucleation of the new phase. For isothermal transformation we have:

$$\psi = \psi_0 + (\bar{\psi} - \psi_0)\left(1 - e^{-(t/\tau)^n}\right) \qquad (1)$$

Here $\tau(T)$ and $n(T)$ are material parameters, which depend on the temperature T, $\bar{\psi}(T)$ is the volume fraction, which should be present in an equilibrium situation and ψ_0 is the fraction present at the start of transformation. The rate of change of the fraction, in the case of isothermal transformation, can be found by differentiation:

$$\frac{d\psi}{dt} = (\bar{\psi}-\psi_0)\, n \frac{1}{\tau^n} t^{n-1} e^{-(t/\tau)^n}$$

Assuming, that the rule of additivity is applicable[3], and, that the direction into which the transformation proceeds, does not change, the time t can be eliminated, by using equation (1):

$$t = \tau \sqrt[n]{\ln\left(\frac{\psi_0 - \bar{\psi}}{\psi - \bar{\psi}}\right)}$$

Which yields for the isothermal rate of phase change:

$$\frac{d\psi}{dt}(\psi, T) = (\bar{\psi} - \psi)\frac{n}{\tau}\left\{\ln\left(\frac{\psi_0 - \bar{\psi}}{\psi - \bar{\psi}}\right)\right\}^{\frac{n-1}{n}} \qquad (2)$$

For transformation of austenite to ferrite and pearlite, the material parameters n and τ can be obtained from TTT diagrams. For transformation of ferrite and pearlite to austenite such diagrams are not available.

Heating

Above T_{A1} the phase diagram gives an equilibrium fraction pearlite $\bar{\psi}_p = 0$. The isothermal rate of change of the pearlite fraction is:

$$\frac{d\psi_p}{dt} = -\psi_p \frac{n}{\tau}\left\{\ln\left(\frac{\psi_{p0}}{\psi_p}\right)\right\}^{\frac{n-1}{n}} \qquad (3)$$

The equilibrium fraction ferrite is $\bar{\psi}_\alpha$. Above T_{A3} according to equilibrium $\bar{\psi}_\alpha$ is zero.

However, as long as not all the pearlite has been transformed to austenite, there is not sufficient carbon available to transform ferrite to austenite according to its equilibrium contents. Therefore the phase rate equation has to be suitably modified. If still ψ_p pearlite is present, the equilibrium fraction ferrite has to be corrected for the carbon deficiency.

$$\bar{\psi}_{\alpha s} = \bar{\psi}_\alpha + \left(\frac{\psi_{\alpha 0} - \bar{\psi}_\alpha}{\psi_{p0}}\right)\psi_p$$

The index s stands for superheating. The difference between volume fraction and mass fraction is neglected. Substitution in (1) yields:

$$\psi_\alpha = \psi_{\alpha 0} + (\bar{\psi}_{\alpha s} - \psi_{\alpha 0})\left(1 - e^{-(t/\tau)^n}\right)$$

and

$$\frac{d\psi_\alpha}{dt} = -(\psi_\alpha - \bar{\psi}_{\alpha s})\frac{n}{\tau}\left\{\ln\left(\frac{\psi_{\alpha 0} - \bar{\psi}_{\alpha s}}{\psi_\alpha - \bar{\psi}_{\alpha s}}\right)\right\}^{\frac{n-1}{n}} + \frac{d\bar{\psi}_{\alpha s}}{dt}\frac{\psi_{\alpha 0} - \psi_\alpha}{\psi_{\alpha 0} - \bar{\psi}_{\alpha s}} \qquad (4)$$

where

$$\frac{d\bar{\psi}_{\alpha s}}{dt} = \left(\frac{\psi_{\alpha 0} - \bar{\psi}_{\alpha}}{\psi_{p0}} \right) \frac{d\psi_p}{dt}$$

Upon reaching a temperature of approximately 910 °C the remaining ferrite will transform to austenite with a low carbon contents. By diffusion the carbon concentration will level out and the austenite is homogenized[4].

Cooling

Because either the temperature was too low, or the time for homogenization was too short, locally low carbon austenite may still be present, when cooling starts. Since no carbon diffusion is required, this will instantaneously transform back to ferrite, when the temperature drops below 910°C. Therefore it is necessary to distinguish between low and high carbon austenite. Here this is done by treating the low carbon austenite as superheated ferrite.

As long as $\psi_{\alpha} > \bar{\psi}_{\alpha}$, equation (4) must be used for the transformation of ferrite to austenite. When the material is cooled below T_{A3}, the current ferrite fraction will drop below the equilibrium fraction and the back transformation from austenite to ferrite will start.

The TTT diagrams as found in steel hardening handbooks are valid for cooling of steel, which has been fully homogenized in the austenitic temperature range. Transformation times of non homogeneous austenite to ferrite and pearlite will be considerably shorter. There is less delay due to nucleation and already some transformation product is formed.

The transformation of homogeneous austenite back to ferrite and pearlite ideally starts with ferrite and pearlite contents $\psi_{\alpha 0} = \psi_{p0} = 0$. Use equation (2), with $\psi_{\alpha 0} = 0$:

$$\frac{d\psi_{\alpha}}{dt} = -(\psi_{\alpha} - \bar{\psi}_{\alpha}) \frac{n}{\tau} \left\{ \ln\left(\frac{\bar{\psi}_{\alpha}}{\psi_{\alpha} - \bar{\psi}_{\alpha}} \right) \right\}^{\frac{n-1}{n}}$$

This way it is automatically taken into account, that transformation of nonhomogeneous austenite proceeds without delay.

2.2. Martensite transformation

The transformation of austenite to martensite is not diffusion controlled, but rather is an instantaneous change of crystal structure. The amount of martensite formed, depends only on temperature.

$$\psi_m = \psi_{\gamma ms} \left(1 - e^{-\beta(T_{ms}-T)} \right) \qquad \text{for } T < T_{ms}$$

Here ψ_m is the volume fraction martensite, $\psi_{\gamma ms}$ is the amount of austenite, that is still present when the Ms temperature T_{ms} is reached. As well T_{ms}, as β depend on the chemical composition. The rate of change of the martensite fraction can then be expressed as:

$$\frac{d\psi_m}{dt} = -\beta \psi_{\gamma ms} e^{-\beta(T_{ms}-T)} \frac{dT}{dt}$$

or, in terms of current fraction contents:

$$\frac{d\psi_m}{dt} = -\frac{d\psi_{\gamma}}{dt} = -\beta \psi_{\gamma} \frac{dT}{dt} \qquad (5)$$

where ψ_{γ} is the current austenite fraction.

3. TEMPERATURE CALCULATIONS

The equation of conservation of energy, neglecting heat production due to deformations, is:

$$\underline{\nabla} \cdot (\underline{\underline{\lambda}} \cdot \underline{\nabla} T) - \rho \dot{e} = 0 \qquad (6)$$

Here $\underline{\underline{\lambda}}$ is the second order tensor of conductivity, ρ is the mass density and e is the specific internal energy. The internal energy is a summation of the energy per fraction.

$$e = \sum_k \psi^k e^k$$

Per fraction the internal energy is a function of the temperature.

$$e^k(T) = \int_{T_o}^{T} c_p^k(T)\, dT + r_o$$

where c_p^k is the specific heat of the k^{th} phase. So the rate of internal energy is:

$$\rho \dot{e} = \sum_k \rho^k \psi^k c_p^k \dot{T} + \sum_k \rho^k \dot{\psi}^k e^k \qquad (7)$$

The first term is the regular specific heat, the second term is a model of latent heat of phase transformation.

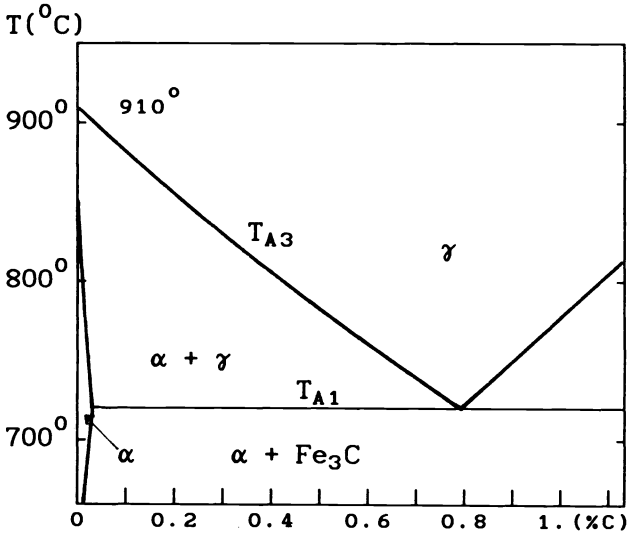

Fig. 1. Equilibrium phase diagram Fe-C

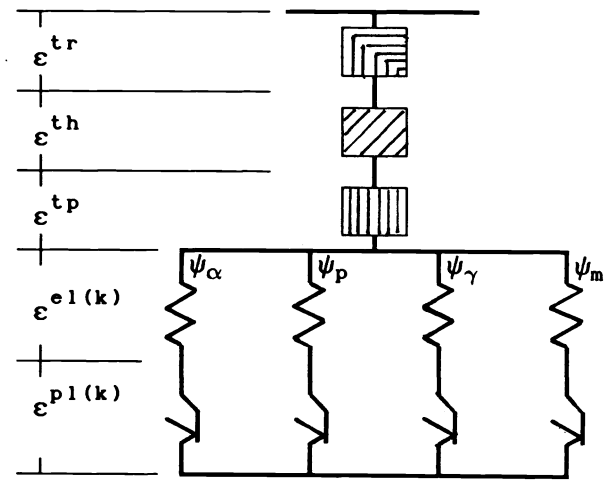

Fig. 2. Parallel fraction model

4. STRESS CALCULATIONS

The calculation of stresses due to quenching has been studied by a number of researchers[5,6]. Only the important equations will be repeated here.
The equilibrium equation in the absence of inertia and body forces, can be written as:

$$\underline{\underline{\sigma}} \cdot \underline{\nabla} = 0 \qquad (8)$$

Here $\underline{\underline{\sigma}}$ is the stress tensor. The stresses depend on the strains and the strain depends on the displacements:

$$\underline{\underline{\varepsilon}} = \tfrac{1}{2} (\underline{u}\, \underline{\nabla} + \underline{\nabla}\, \underline{u}) \qquad (9)$$

The strain tensor $\underline{\underline{\varepsilon}}$ is assumed to consist of a number of independent contributions:

$$\underline{\underline{\varepsilon}} = \underline{\underline{\varepsilon}}^{el} + \underline{\underline{\varepsilon}}^{pl} + \underline{\underline{\varepsilon}}^{th} + \underline{\underline{\varepsilon}}^{tr} + \underline{\underline{\varepsilon}}^{tp}$$

where $\underline{\underline{\varepsilon}}^{el}$ is the elastic part, $\underline{\underline{\varepsilon}}^{pl}$ is the plastic strain, $\underline{\underline{\varepsilon}}^{th}$ is the thermal dilatation, $\underline{\underline{\varepsilon}}^{tr}$ is the strain due to phase transformation and $\underline{\underline{\varepsilon}}^{tp}$ is due to transformation plasticity. The last two are specific for phase transformation calculations and will be treated in some detail.

4.1. Transformation (and thermal) strain

The mass density can be written as a weighted sum of the phase fractions.

$$\rho = \sum_k \psi^k \rho^k$$

The mass density ρ^k of each phase is a function of temperature.

$$\frac{d\rho}{dt} = \sum_k \frac{d\psi^k}{dt} \rho^k + \sum_k \psi^k \frac{d\rho^k}{dT} \frac{dT}{dt}$$

The first term on the right hand side is the density change due to phase transformation, the second term, due to thermal expansion. For isotropic materials, density change and lineal strain ε are related by:

$$d\varepsilon = -\frac{1}{3} \frac{d\rho}{\rho}$$

The strain rates due to phase transformation and thermal expansion are:

$$\dot{\underline{\underline{\varepsilon}}}^{tr} = -\frac{1}{3} \sum_k \frac{\rho^k}{\rho} \frac{d\psi^k}{dt} \underline{\underline{I}} \qquad (10)$$

$$\dot{\underline{\underline{\varepsilon}}}^{th} = -\frac{1}{3} \sum_k \frac{\psi^k}{\rho} \frac{d\rho^k}{dT} \frac{dT}{dt} \underline{\underline{I}} = \sum_k \psi^k \frac{\rho^k}{\rho} \alpha^k \frac{dT}{dt} \underline{\underline{I}} \qquad (11)$$

Here $\underline{\underline{I}}$ is the second order unit tensor and α^k is the coefficient of thermal expansion of phase k.

4.2. Transformation plasticity

Experiments show[7], that applying a stress, while phase transformation occurs, results in a permanent strain, which can not be explained from yielding of one of the phases involved. A qualitative description can be obtained by considering stress relaxation in the transformed phase.
For low stress levels, this strain is found to be proportional to the applied stress and to the amount of phase transformed. The usual generalization[8] to a multi-axial stress state expresses the transformation plasticity proportional to the deviator stress $\underline{\underline{s}}$.

$$\underline{\underline{s}} = \underline{\underline{\sigma}} - \tfrac{1}{3}\mathrm{tr}(\underline{\underline{\sigma}})\, \underline{\underline{I}}$$

$$\dot{\underline{\underline{\varepsilon}}}^{tp} = \tfrac{3}{2} K \frac{d\psi}{dt} \underline{\underline{s}} \qquad (12)$$

The constant K depends on the chemical composition of the material involved, on the type of transformation and on the direction, into which the transformation proceeds.

4.3. Constitutive stress-strain equations

The stress rate is assumed proportional to the elastic strain rate.

$$\dot{\underline{\underline{\sigma}}} = \underline{\underline{\underline{\underline{E}}}} : \dot{\underline{\underline{\varepsilon}}}^{el} + \dot{\underline{\underline{\underline{\underline{E}}}}} : \underline{\underline{\varepsilon}}^{el} = \underline{\underline{\underline{\underline{E}}}} : (\dot{\underline{\underline{\varepsilon}}} - \dot{\underline{\underline{\varepsilon}}}^{pl} - \dot{\underline{\underline{\varepsilon}}}^{tp} - \dot{\underline{\underline{\varepsilon}}}^{th} - \dot{\underline{\underline{\varepsilon}}}^{tr}) + (\dot{\underline{\underline{\underline{\underline{E}}}}} : \underline{\underline{\underline{\underline{E}}}}^{-1}) : \underline{\underline{\sigma}}$$

The description of plastic deformation is based on the Von Mises yield criterion, with isotropic hardening. Plastic deformation will occur when the deviator stress exceeds the yield surface, which depends on the one dimensional yield stress σ_y.

$$\Phi(\underline{\underline{s}}, \varepsilon^p, T) = \underline{\underline{s}} : \underline{\underline{s}} - \frac{2}{3}\sigma_y^2(\varepsilon^p, T) = 0$$

Using classical flow theory for plasticity, the plastic strain rate is given by:

$$\dot{\underline{\underline{\varepsilon}}}^{pl} = \frac{3}{2}\frac{\dot{\varepsilon}^p}{\sigma_y}\underline{\underline{s}}$$

The equivalent plastic strain rate $\dot{\varepsilon}^p$ is defined by:

$$\dot{\varepsilon}^p = \sqrt{\frac{2}{3}\dot{\underline{\underline{\varepsilon}}}^{pl} : \dot{\underline{\underline{\varepsilon}}}^{pl}}$$

After solving for the plastic strain rate, an expression for the stress rate is found:

$$\dot{\underline{\underline{\sigma}}} = \left(\underline{\underline{\underline{\underline{E}}}} - (1 - \frac{1}{3}\frac{1}{G}\frac{\partial\sigma_y}{\partial\varepsilon^p})\frac{3G\,\underline{\underline{s}}\,\underline{\underline{s}}}{\sigma_y^2} \right) : \dot{\underline{\underline{\varepsilon}}} + \sum_k \left(\frac{1}{3}\frac{\rho^k}{\rho} 2G \frac{1+\nu}{1-2\nu}\underline{\underline{I}} - \frac{\partial\sigma_y}{\partial\varepsilon^p}K^k\,\underline{\underline{s}} \right)\dot{\psi}^k +$$

$$+ \left\{ \frac{1}{3}\sum_k \frac{\psi^k}{\rho}\frac{d\rho^k}{dT} 2G\frac{1+\nu}{1-2\nu}\underline{\underline{I}} + \left(\frac{d}{dT}\left(\underline{\underline{\underline{\underline{E}}}}\right) : \underline{\underline{\underline{\underline{E}}}}^{-1}\right) : \underline{\underline{\sigma}} + (1 - \frac{1}{3}\frac{1}{G}\frac{\partial\sigma_y}{\partial\varepsilon^p})\frac{2G\underline{\underline{s}}}{\sigma_y}\frac{\partial\sigma_y}{\partial T} \right\}\dot{T} \qquad (13)$$

Where G is the shear modulus and ν is Poisson's ratio. The stress rate is found to be composed of three terms, a strain rate dependent part, a phase transformation dependent part and a temperature rate dependent part.
More than one phase may be present simultaneously. Then it is not justified to use this macroscopic expression for the stress rate. Each phase has different elasticity coefficients, yield stress and hardening modulus.
A different stress for each phase is assumed and the macroscopic stress is written as a weighted sum of the stress per phase:

$$\underline{\underline{\sigma}} = \sum_k \psi^k\,\underline{\underline{\sigma}}^k$$

A material model is constructed, where the transformation plasticity, the thermal expansion and the transformation induced strain are macroscopic and the elastic and plastic strains are evaluated per phase fraction (Fig. 2.).
The constitutive equations for the different phases are modified accordingly.

5. FINITE ELEMENT DISCRETIZATION

Following Galerkin's method, the mechanical and the thermal equilibrium equations (8) and (6) are written in the weak form. After applying the divergence theorem and disregarding surface tractions we find:

$$\int_V \underline{\nabla}\,\underline{v} : \dot{\underline{\underline{\sigma}}}\,dV = 0 \qquad (14a)$$

$$\int_V \left(\underline{\nabla}\,\theta \cdot \underline{\underline{\lambda}} \cdot \underline{\nabla}\,T + \theta\,\rho\,\dot{e} \right) dV + \int_S \theta\,\varphi\,dS = 0 \qquad (14b)$$

where $\underline{v}$ and θ are virtual velocity and virtual temperature fields, φ is the heat flow through the surface S of the body and V is the volume of the body. Substitution of (7), (9) and (13) yields an expression in the velocities $\dot{\underline{u}}$ and $\underline{v}$, the temperatures T and θ and the phase composition ψ.
The body is divided into finite elements. In each element the velocity and temperature fields are approximated by interpolation between unknown nodal point values, which are gathered in the arrays $\{\dot{U}\}$ and $\{\dot{T}\}$. After carrying out the appropriate

integrations and requiring that (14) holds for all values of $\underline{v}$ and θ, we find a set of algebraic equations in the components of $\{ \dot{U} \}$ and $\{ \dot{T} \}$.

$$\begin{bmatrix} [K] & [R] \\ - & [B] \end{bmatrix} \begin{Bmatrix} \dot{U} \\ \dot{T} \end{Bmatrix} = \begin{Bmatrix} \{F(\dot{\psi})\} \\ -[\Lambda]\{T\} - \{Q(\dot{\psi})\} - \{\Phi\} \end{Bmatrix} \tag{15}$$

The first row is the discrete version of equation (14a). The sub-matrix [K] is the stiffness matrix, [R] is the thermo-mechanical coupling matrix containing the thermal expansion terms and the temperature dependence of the mechanical properties. The vector {F} represents the dilatation due to phase transformation.
The second row corresponds to equation (14b). The matrix [B] is the heat capacity matrix, [Λ] is the heat conduction matrix, the vector {Q} contains the latent heat due to phase transformation and {Φ} is the heat flow through the surface.

5.1. Incremental Solution Procedure

After multiplication of the rate equation (15) by the time step Δt, we obtain an incremental formulation in $\{\Delta U\}$ and $\{\Delta T\}$. The right-hand side is evaluated at time $\tilde{t} = t + \frac{1}{2}\Delta t$. The extra terms with $\{\Delta T\}$ are then included in the sub-matrices [R] and [B]. This way an implicit formulation is obtained.

$$\begin{bmatrix} [K] & [R^*] \\ - & [B^*] \end{bmatrix} \begin{Bmatrix} \Delta U \\ \Delta T \end{Bmatrix} = \begin{Bmatrix} \{F(\dot{\psi})\} \\ -[\Lambda]\{T\} - \{Q(\dot{\psi})\} - \{\tilde{\Phi}\} \end{Bmatrix} \tag{16}$$

The matrices $[R^*]$ and $[B^*]$ are evaluated as:

$$[R^*] = [R] - \tfrac{1}{2}[F(\frac{\partial}{\partial T}\dot{\psi})]$$

$$[B^*] = [B] + \tfrac{1}{2}[\Lambda] + \tfrac{1}{2}[Q(\frac{\partial}{\partial T}\dot{\psi})] + \tfrac{1}{2}[\frac{\partial}{\partial T}\Phi]$$

A solution for $\{\Delta u\}$ and $\{\Delta T\}$ is sought by iteration until equilibrium is reached. The matrices [K], $[R^*]$ and $[B^*]$ are updated at the start of each iteration.

6. APPLICATION

The theory as outlined here is demonstrated by a simulation of the hardening of a central spot on a steel disk. The simulation is accompanied by an experiment and the results of both are compared.
The laser is a 1540 W CO_2 laser. The beam diameter at the specimen is 8 mm.
A 10 mm thick slice is cut from a cylindrical bar with diameter 40 mm. The material is commercially available steel C45. No heat treatment is applied prior to laser treatment. The surface is coated with graphite to enhance optical efficiency.
A number of different interaction times were used. It was found, that melting of the surface layer occurred after 0.7 seconds exposure.
The simulation is carried out on a model, consisting of a 11x10 mesh of axi-symmetric four node elements. The mesh is biased towards the center of the spot.
The total simulation was done in 150 time steps, each requiring 3 or 4 equilibrium iterations. The run time was approximately 20 hr on a μVax 2000 computer.
The four phases each have different temperature dependent mechanical and thermal properties (Table 1).
The optical efficiency of the surface is assumed 70 %, which yields a total power of 1200 W. The distribution of the power over the beam area is assumed constant.
In the simulation the melting temperature was reached after 0.6 sec heating.
The results of the calculation with interaction time 0.6 s are presented here and

material properties		ferrite/pearlite	austenite	martensite
Youngs modulus	20 °C	210 GPa	200 GPa	200 GPa
	600 °C			50 GPa
	1500 °C	90 GPa	50 GPa	
Yield stress	20 °C	360 MPa	190 MPa	1600 MPa
	600 °C	40 MPa	30 MPa	1250 MPa
	1500 °C	10 MPA	10 MPa	
Specific density	20 °C	7850 kg/m^3	8000 kg/m^3	7760 kg/m^3
	600 °C			7575 kg/m^3
	1500 °C	7300 kg/m^3	7300 kg/m^3	
Specific heat	20 °C	480 J/kgK	480 J/kgK	480 J/kgK
	1500 °C	900 J/kgK	900 J/kgK	900 J/kgK
Conductivity	20 °C	49 W/mK	15 W/mK	40 W/mK
	600 °C			30 W/mK
	1500 °C	25 W/mK	25 W/mK	

Table 1. Material properties for simulation of laser hardening

are compared to the results of a test with the same interaction time.
Figures 3 and 4 show the temperature history and the phase fraction history of two points, one on the surface and the other at a depth of 0.44 mm. In Fig. 5 the eventual martensite concentration is compared to a microscopic picture of the heat affected zone. The martensite fraction as calculated is shown compared with measured hardness values in Fig. 6. The extent of the heat affected zone is shown in Fig. 7. The diameter of the martensite zone in the test was approximately 6.2 mm.
From the comparison of calculations with measurements it appears, that in the simulation the amount of martensite is slightly overestimated. The overall picture however compares surprisingly well.

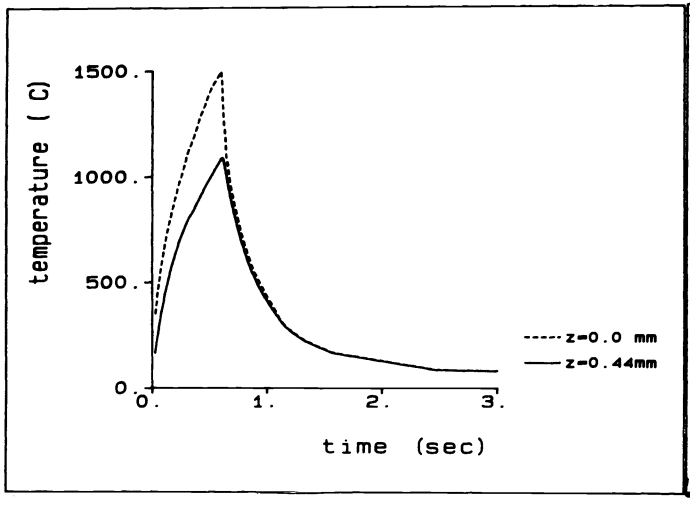

Fig. 3. Thermal cycle of two points, one at and one 0.44mm below the surface.

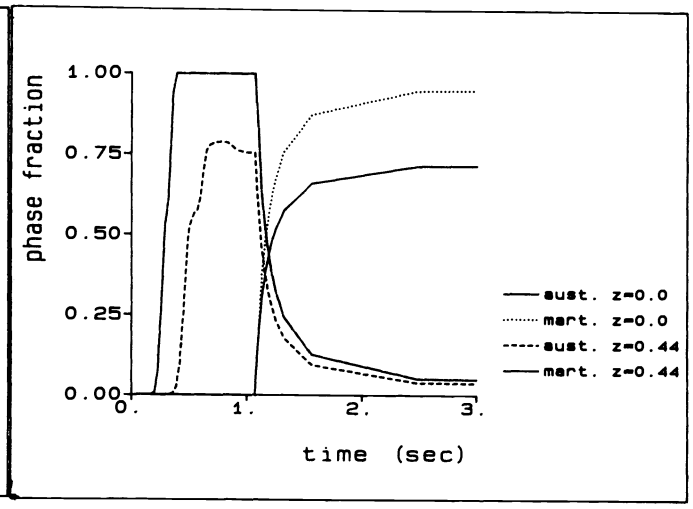

Fig. 4. Phase fraction history at the surface and 0.44 mm below the surface

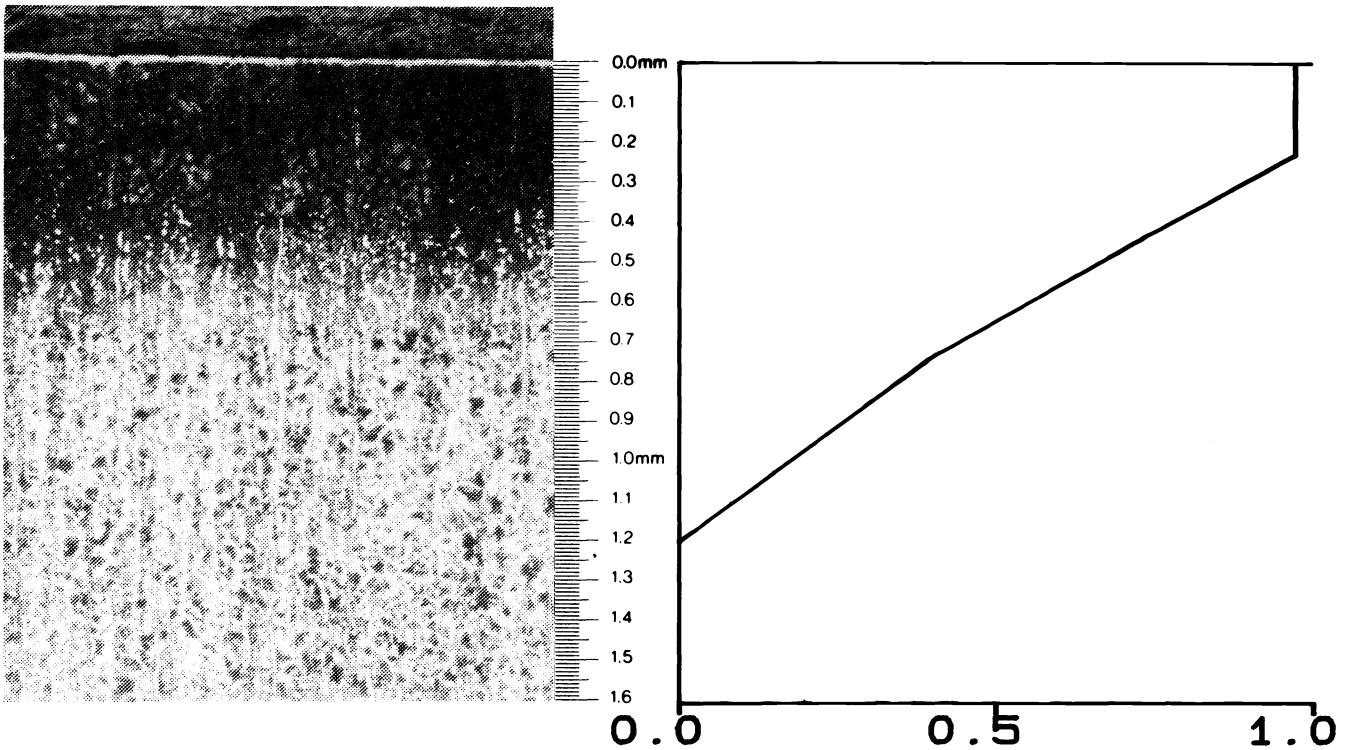

Fig. 5. Comparison of the calculated martensite fraction with microscope picture of the heat affected zone.

The plot of the deformations (Fig. 8) shows the typical convexity of the treated surface, with a slight raise (≈ 12 μm) of the heat affected zone. The residual radial stress at the center line (Fig. 9) also shows the typical pattern[9,10] of a small compression zone at the surface and high tension stresses just below the heat affected zone. The Absolute values of the stress however are at least twice as high

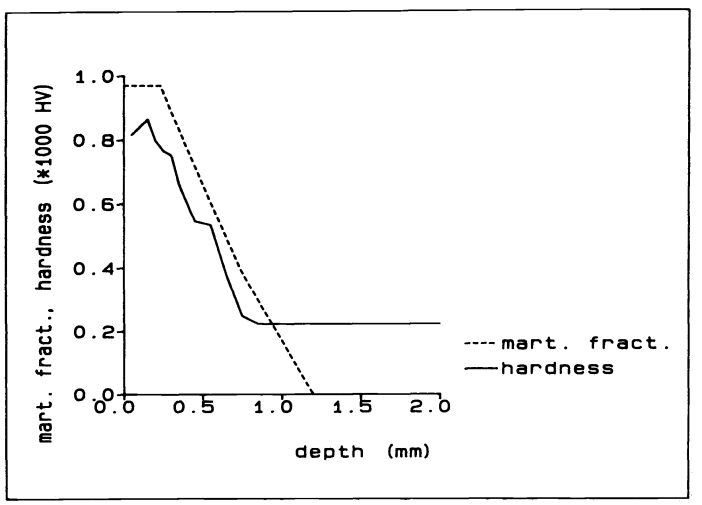

Fig. 6. Comparison of calculated martensite fraction with measured hardness data (HV300)

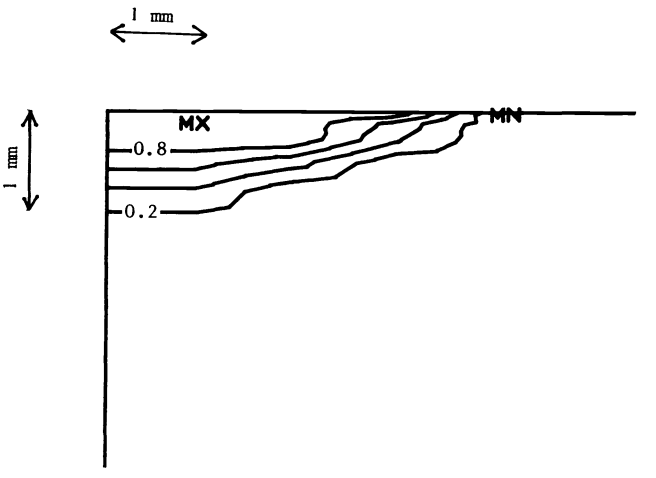

Fig. 7. The distribution of the martensite fraction in the heat affected zone

as reported in the literature[9]. This is mainly due to the fact that the stress state is axi-symmetric, rather than two-dimensional. Furthermore, the work hardening rule as employed here tends to predict rather high yield stresses when the plastic strain is high.

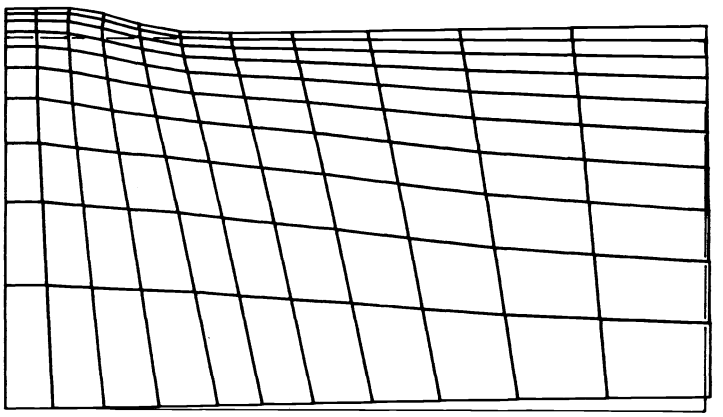

Fig. 8. Deformation of the heat treated disc after cooling down

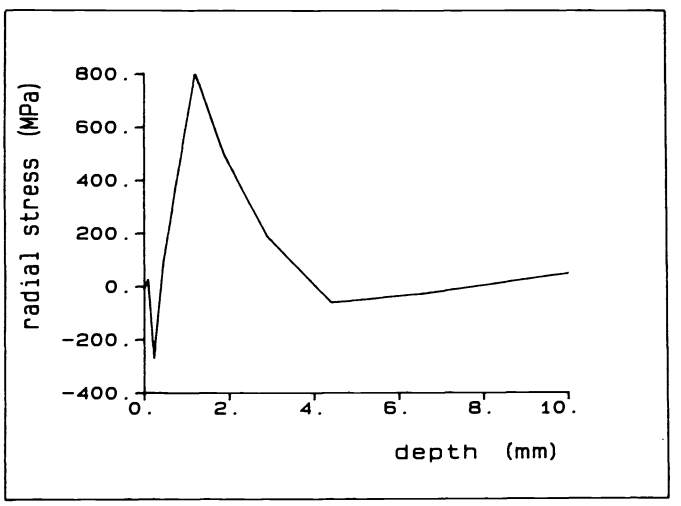

Fig. 9. Residual radial stress at the center line

7. CONCLUSIONS

The possibilities to use finite elements for the calculation of temperatures, phase contents, deformations and stresses during laser heat treatment are demonstrated. In order to perform reliable simulations, mechanical as well as thermodynamic properties of the constituent phases are required at room temperature and at

elevated temperatures.
Simulation of the three dimensional case of a scanning laser beam is not yet feasible, keeping in mind the computational effort required.

8. ACKNOWLEDGMENTS

The authors wish to thank Ipe van Sprang for carrying out the laser treatments and Peter Vreede and Marcel Louwes for assistance with programming.

9. REFERENCES

1. R. Chatterjee-Fischer, R. Rothe, R. Becker: "Überblick über das Härten mit dem Laserstrahl", *Haerterei Techn. Mitt.* Vol. 39 (1984) 91-98.
2. M. Avrami: "Kinetics of Phase Change", *J. Chem. Phys.*, vol. 7 (1939), 1103-1112; Vol. 8 (1940) 212-224; Vol. 9 (1941) 177-184.
3. J.W. Cahn: "Transformation Kinetics during Continuous Cooling", *Acta Metall.*, Vol. 7 (1959) 572-575.
4. M.F. Ashby, K.E. Easterling: "The Transformation Hardening of Steel Surfaces by Laser Beams I Hypo-eutectoid Steels", *Acta Metall.*, Vol. 32 (1984) 1935-1948.
5. S. Denis, S. Sjöström, A. Simon: "Coupled Temperature, Stress, Phase Transformation Model", In: "*Residual Stresses in Science and Technology*", ed. E. Macherauch, V. Hauk, (1986) 595-602.
6. T. Inoue, "Description of Transformation Kinetics, Heat Conduction and Elasto-Plastic Stress in the course of Quenching and Tempering of some Steels", *Ingenieur Archiv*, Vol. 50 (1981) 315-327.
7. M. de Jong, G.W. Rathenau: "Mechanical Properties of Iron and some Iron Alloys while undergoing Allotropic Transformation", *Acta Metall.*, Vol 7 (1959) 246-253.
8. S. Denis, A. Simon: "The Role of Transformation Plasticity in the Calculation of Quench Stresses in Steel", In: "*Residual Stresses in Science and Technology*", ed. E. Macherauch, V. Hauk, (1986) 565-572.
9. A. Solina, M. De Sanctis, L. Paganini, A. Blarasin, S. Quaranta: "Origin and Development of Residual Stresses Induced by Laser Surface Hardening Treatments", *J. Heat Treating*, Vol 3 (1984) 193-204.
10. D. Grevey, L. Maiffredy, A.B. Vannes: "A Simple way to Estimate the level of the Residual Stresses after Laser Heating", *J. Mech. Working Techn.*, Vol 16 (1988) 65-78.